Vehicle System Dynamics
International Journal of Vehicle Mechanics and Mobility

ISSN: 0042-3114 (Print) 1744-5159 (Online) Journal homepage: www.tandfonline.com/journals/nvsd20

Investigation on the safety of 30,000-ton combined train with different lag times of slave control locomotives

Qun Ma, Wei Wei, Yuan Yao & Xinmiao Chen

To cite this article: Qun Ma, Wei Wei, Yuan Yao & Xinmiao Chen (2026) Investigation on the safety of 30,000-ton combined train with different lag times of slave control locomotives, Vehicle System Dynamics, 64:2, 302-325, DOI: 10.1080/00423114.2024.2432386

To link to this article: https://doi.org/10.1080/00423114.2024.2432386

Published online: 23 Nov 2024.

VEHICLE SYSTEM DYNAMICS
2026, VOL. 64, NO. 2, 302–325
https://doi.org/10.1080/00423114.2024.2432386

Investigation on the safety of 30,000-ton combined train with different lag times of slave control locomotives

Qun Ma[a], Wei Wei[b], Yuan Yao [a,c] and Xinmiao Chen[a]

[a]State Key Laboratory of Rail Transit Vehicle, Southwest Jiaotong University, Chengdu, People's Republic of China; [b]College of Locomotive and Rolling Stock Engineering, Dalian Jiaotong University, Dalian, People's Republic of China; [c]State Key Laboratory of Heavy-Duty and Express High-Power Electric Locomotive, Zhuzhou, People's Republic of China

ABSTRACT

To investigate the influence of the lag time in braking response of the slave control locomotives caused by the LOCOTROL wireless synchronous control system on the longitudinal impulse of the train, a 30,000-ton heavy-haul train model was established. The model is in the form of '1+1+1+1'. The simulation accuracy of the air braking system was verified by comparing with static tests. A dynamic model consisting of two HXD1 locomotives and a 100-type couple was established for study the middle locomotive's running safety. Results show that, under normal transmission delays, the lag time in the braking response of the slave control locomotives is approximately 2–3 s. The lag time significantly influence the coupler force and its distribution law. During emergency braking, the lag time increased from 0 s to 6 s, and the maximum coupler force increased by 1877.1 kN. Among the three slave control locomotives, the one positioned in the middle has the greatest impact on the coupler force, while the one closest to the leading locomotive has the least impact. When the lag time reaches 5 s, the middle locomotive's coupler becomes unstable. Increasing the lateral stiffness of the secondary suspension is beneficial for enhancing the locomotive's ability to stabilise the coupler.

ARTICLE HISTORY
Received 20 March 2024
Revised 13 November 2024
Accepted 16 November 2024

KEYWORDS
30,000-ton combined train; longitudinal dynamic; coupler stability; lag time; slave control locomotive

1. Introduction

Heavy-haul railway transportation has the advantages of large capacity, low cost, energy saving and environmental protection, and has gradually attracted extensive attention from all countries. In recent years, China has promoted the transportation strategy of 'shifting from highways to railways', which has led to a continuous increase in the demand for heavy-haul railways. In order to increase the transportation capacity on heavy-haul railways in China, the Shuohuang Railway is actively preparing for the operation of 30,000-ton combined trains. In the near future, the 30,000-ton combined trains will replace the current 20,000-ton combined trains operating in China.

Years of research on the longitudinal dynamics of heavy-haul trains show that the coupler force will increase significantly after the train is lengthened. Therefore, the problem

CONTACT Yuan Yao yyuan8848@163.com

of coupler force must be addressed first in the operation of the 30,000-ton combined train. This problem has always been the bottleneck of the development of heavy-haul trains.

There are several main factors that affect the coupler force of trains, such as the transmission delay of the LOCOTROL wireless synchronous control system, marshalling mode, operation method, line condition, locomotive traction and electric braking characteristics [1]. The different starting times of vehicle braking along the length of the train are one of the main reasons for the longitudinal impulse. In order to solve this problem, the LOCOTROL wireless synchronous control system is applied to the 30,000-ton combined train, and a slave control locomotive (SCL) is added at the rear of the train [2], which makes the synchronisation of the train significantly improve during braking and release. Due to the transmission delay effect of the LOCOTROL system [3], the braking sources (three SCLs) located at different positions of the train have different lag times (LTs) when transmitting the braking signal.

An emergency braking stop test was conducted on the K129 flat track of Daqin Line for a 20,000-ton combined train in the form of 'SS4+102∗C80+2∗SS4+102∗C80+SS4(1+2+1)' marshalling. The maximum coupler force reached 2276 kN. After analysis, the main reason is that the middle SCL and the tail SCL started emergency braking after the lead locomotive braked for 6.1 s [4]. Shortly after the test, at K141.8 of Daqin line, the derailment accident of a 20,000-ton combined train with '1+2+1' marshalling was also caused by similar reasons. With the increase in the number of SCL, the influence of braking delay of multiple braking sources on the longitudinal impulse of the 30,000-ton combine train is unknown. Therefore, it is particularly necessary to study the influence of transmission delay between the leading locomotive and the SCLs on train operation safety by simulation calculation before train operation.

It is worth noting that the middle SCL is located in the high-force section of the train's longitudinal characteristics and often bears the greatest longitudinal impulse. When the compression coupler force exceeds the friction limit, the coupler will be unstable and produce a large lateral swing. The instability of the coupler will deteriorate the service performance of the coupler and draft gear, which can easily lead to serious faults such as coupler crack, coupler separation, and draft gear failure. In addition, the angle of the coupler, from curving or instability, causes the coupler force to producing lateral forces on the car body, resulting in the lateral dislocation of the car body and even train derailment [5]. Therefore, it is of great theoretical and practical significance to study the longitudinal impulse and coupler stability of the 30,000-ton combined train. Note that this paper primarily focuses on the influence of train braking characteristics on longitudinal impulse, without considering the SCLs command delay, and only analyses the longitudinal impulse caused by the LT of the SCLs' braking response.

1.1. Available literature

With the increase in the length of heavy-haul trains, the problem of train longitudinal impulse and coupler instability has become more and more prominent, leading makes many scholars devote to themselves to studying these problems. Rao [6] established a mathematical model early on and studied the transient response of train coupler force under different locomotive operation modes. Geike [7] analysed coupler forces during multi-train coupling using the established unitised combined train model. Belforte [8] used MATLAB simulation software to simulate the longitudinal dynamics of heavy-haul railways in Europe and explored the impact of different marshalling modes on the safety of train operation. Cole et al. [9] proposed a co-simulation method of locomotive traction control, vehicle system dynamics and train longitudinal dynamics, and carried out experimental verification. Wei et al. [10,11] developed the Train Air Brake and Longitudinal Dynamics Simulation System, which is widely used in the fields of train longitudinal dynamics analysis, air brake system structure optimisation, accident analysis, and operation optimisation. Simson and Cole [12] proposed a calculation method for coupler lateral swing angle, considering the coupler force.

Luo and Ma [13–15] were the first to address the problem of coupler stability under compression for the issue of locomotive derailment in the middle of heavy-haul train on the Daqin line, and put forward two kinds of coupler modelling methods and coupler stability mechanisms. Yao et al. [16–18] researched the stability and mechanical properties of the 102-type coupler, analysed the geometric shape and force state of the couplers under different deflection angles and longitudinal forces, and summarised the structural characteristics of the couplers. Meanwhile, based to the different structural characteristics and stability mechanism of the two couplers, a new coupler was proposed. Wang et al. [19,20] conducted simulation and field test research on the 100-type coupler, and proposed a scheme to improve the stability of 100-type coupler by using smaller secondary lateral stop clearance.

1.2. Scope of the paper

After a comprehensive literature review, it is clear that the above research has greatly enriched the research in the fields of longitudinal impulse and coupler stability of heavy-haul trains. However, there are few reports on the study of the longitudinal impulse of 30,000-ton combined trains, and no relevant research has been conducted on the feasibility of applying the 100-type coupler to 30,000-ton combined trains. Therefore, the main purpose of this paper is to address and fill these gaps in the existing literature. This paper can provide references for the safe operation of the 30,000-ton combined trains on the Shuohuang Railway in China.

The main contents of this paper are as follows: Section 2 introduces the modelling method of the train longitudinal dynamics, including the simulation principle of the air brake system. In Section 3, the accuracy of the established train model is verified by comparing the static test and simulation results. Section 4 introduces the structural characteristics and stability mechanism of the 100-type coupler. Section 5 studies the influence of the LT of the SCLs on the longitudinal impulse of the 30,000-ton combined train is studied. Section 6, the stability of the SCL and its coupler is analysed when the LT of the SCLs is large. Section 7 provides a comprehensive summary of this paper.

2. Modelling of train longitudinal dynamics

2.1. Train air brake and longitudinal dynamics simulation system

The simulation method is the main approach to study the longitudinal impulse of heavy-haul trains. How to describe the characteristics of braking systems during the braking

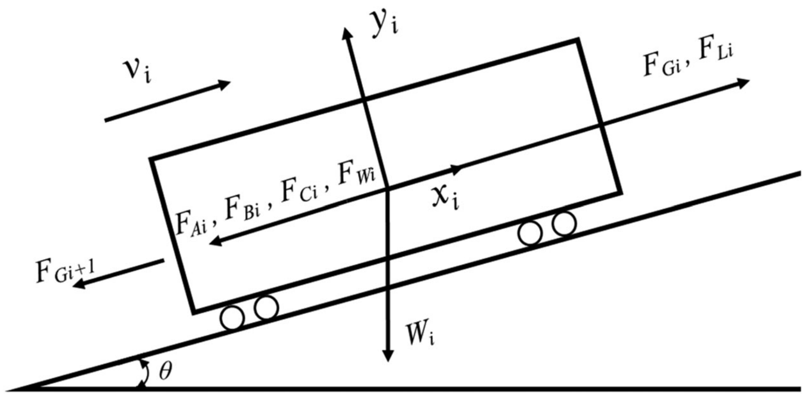

Figure 1. Force diagram of single vehicle.

process using simulation method is the difficulty and hot spot in the present international research. As reviewed by Wu et al. [21], train air brake models can be classified into three categories: empirical [22–24], fluid dynamics [25–27] and fluid-empirical dynamics models [28–30]. In order to obtain more applicable and more accurate characteristics of train air brake systems, this paper adopts the Train Air Brake and Longitudinal Dynamics Simulation System (TABLDSS) developed by Dalian Jiaotong University. TABLDSS is based on the simulation method of air brake systems based on gas flow theory. The simulation system has the ability to simulate various types of locomotives and vehicles running on various line conditions. There is no need to make any assumptions about the brake pipe pressure wave propagation speed or the pressure rise characteristics of the brake cylinder. This overcomes the limitation of braking test data and offer greater adaptability, which is a real numerical simulation of the braking process. In 2017, TABLDSS ranked among the best in international longitudinal dynamic evaluation in terms of calculation accuracy and speed [31]. The simulation system is widely used in China's Daqin Railway and Shuohuang Railway, which already operated 20,000-ton combined trains, and has become a powerful tool for operation method optimisation and accident analysis.

2.2. Train longitudinal dynamics simulation model

In the simulation system, each locomotive (or vehicle) is regarded as a concentrated mass, and each vehicle is connected by a spring-damping unit. The force analysis of any vehicle (locomotive) i is shown in Figure 1.

Each vehicle has the following force equilibrium equation:

$$F_{1i} = F_{Gi} - F_{Gi+1} + F_{Li} - F_{wi} \tag{1}$$

$$Mi\,\alpha i = F1i + F2i \tag{2}$$

$$F_{2i} = \begin{cases} -\dfrac{v_i}{|v_i|}(F_{Ai} + F_{Bi} + F_{Ci}) & v_i > 0 \\ -(F_{Ai} + F_{Bi} + F_{Ci}) & v_i = 0 \quad and \quad F_{1i} \geq (F_{Ai} + F_{Bi} + F_{Ci}) \\ -F_{1i} & v_i = 0 \quad and \quad F_{1i} < (F_{Ai} + F_{Bi} + F_{Ci}) \\ 0 & v_i = 0 \quad and \quad F_{1i} = 0 \end{cases} \tag{3}$$

where $M_i\alpha_i$, F_{Li}, F_{Gi}, F_{Bi}, F_{Ci}, $F_{Ai}$and F_{Wi} are inertia force, traction force or electric braking force, coupler force, air braking force, curve resistance running resistance and grade resistance respectively. M_i, x_i, v_i and i indicate vehicle mass, instantaneous position, speed and serial number, respectively. By solving the equations of equation (2) at any time, the physical state and forced condition of each locomotive and vehicle of the train can be obtained.

According to China Railway Standard and train traction calculation (TB/T 1407.1-2018) [32], the basic running resistances of locomotives and wagons are as follows:

$$\omega_1 = 0.92 + 0.0048v + 0.000125v^2 \tag{4}$$

$$\omega_2 = 1.40 + 0.0038v + 0.00013v^2 \tag{5}$$

Where, w_1 is the basic running resistance of wagons C80 (N/kN) and w_2 is the basic running resistance of locomotive HXD1 (N/kN).

Combined with the test data of heavy-haul trains, the basic running resistance is corrected in the simulation system. The basic resistance model formula of the new full-load operating unit is as follows :

$$\omega_0' = 0.95062 + 0.00114v \tag{6}$$

This formula, derived from tests conducted on the Shuohuang line in China, accurately calculates the basic running resistance of trains on this specific route. Compared with Formula 4, the constant term of this formula is larger, the coefficient of the primary term is smaller, and the quadratic term is omitted. The C80 wagons currently employed on the Shuohuang Railway in China utilise E-class axles, resulting in increased axle load. Consequently, the proportion of air resistance (Cv^2) in the basic running resistance decreases while the constant term increases. Additionally, as the speed decreases, the proportion of air resistance will decrease. Due to the conditions of the Shuohuang Railway, trains on this line have a maximum operating speed of 80 km/h and a maximum speed of 70 km/h on long and steep downhill sections. This will cause the running speed of the train to be in a low range during the entire running process. Relevant test results and simulation results can be found in reference [33].

2.3. Braking system physical model

Figure 2(a) is the train air brake system model, it contains the locomotive braking system and the vehicle braking system. The locomotive braking system has locomotive automatic brake unit (pos.1) and the locomotive independent brake valve (pos.2). The vehicle braking system consists of a train brake pipe (including branch pipe and connecting pipe), a distributing valve (pos.4), a brake cylinder (pos.6), an auxiliary reservoir (pos.5), an acceleration release reservoir (pos.3), an emergency room etc. Because locomotive independent brake valve only control locomotive itself, and it is some what different from the vehicle's, in order to simplify the model. The locomotive independent brake valve is not modelled individually but replaced with the vehicle braking system, which has a special force amplify rate [10].

Figure 2(b) is a model of automatic brake unit. Automatic brake unit includes locomotive handle, main reservoir, equalising reservoir, regulating valve, relay valve, compressor

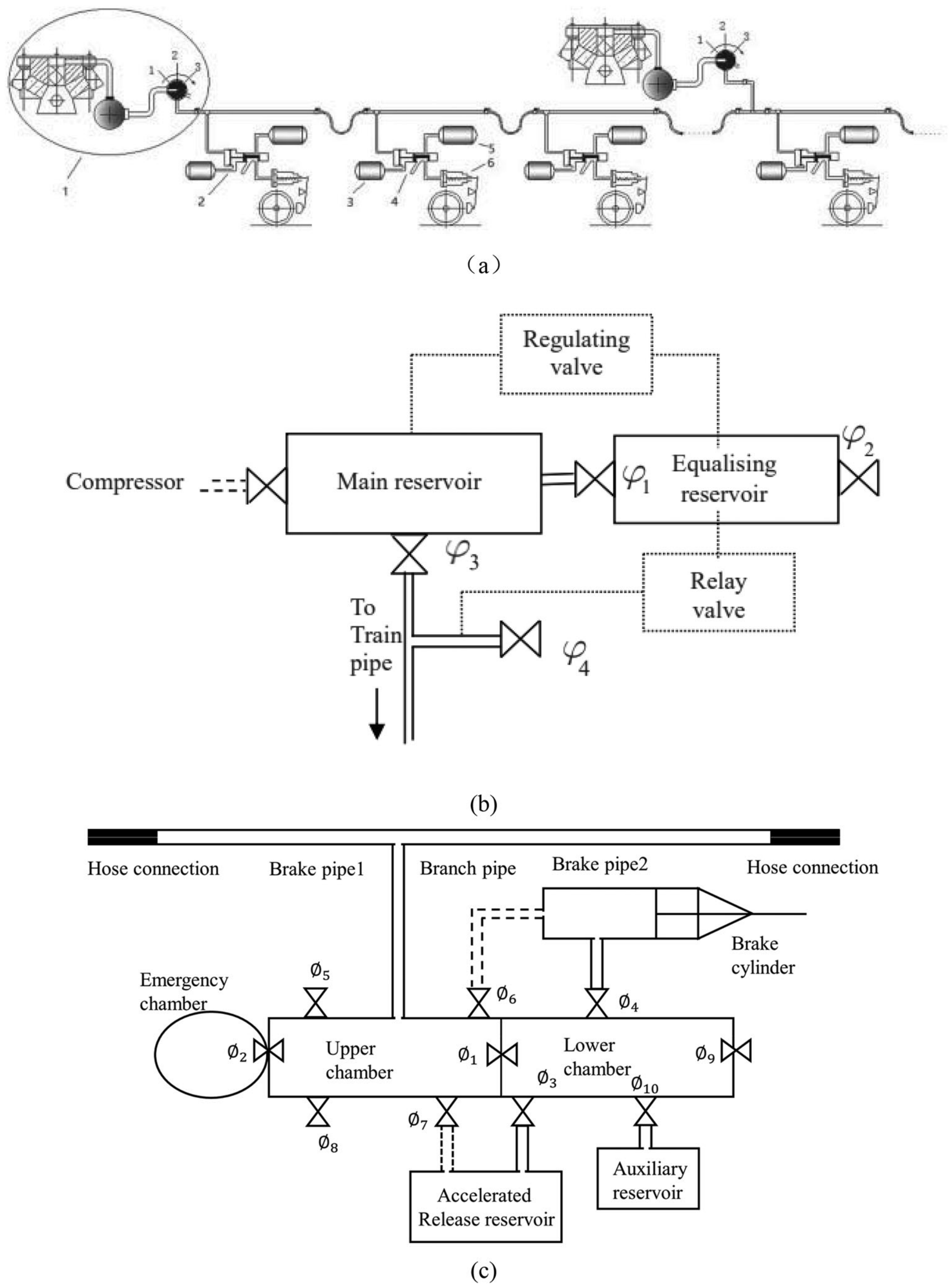

Figure 2. Simulation model of train air brake system (a) Train air brake system. (b) Locomotive automatic brake unit mode. (c) Single vehicle braking system model [10].

and other components. Automatic brake unit is the source of the control signal of the train brake system, so modelling the automatic brake unit is very important. In the model of automatic brake unit, there are one main reservoir, one equalising reservoir, two compressors, one pipe connecting the main reservoir and equalising reservoir, one pipe connecting the main reservoir and brake pipe of train. The regulating valve, relay valve and vent valve are modelled based on their principles to control the open/close and the diameter of orifices $\varphi 1$, $\varphi 2$, $\varphi 3$ and $\varphi 4$.

Figure 2(c) is a single vehicle braking system model. Each vehicle braking system is composed of 6 pipes, 6 chambers and one control unit. Each pipe is connected to the chamber through a valve. The model uses 10 ports to simulate the internal working of the valve. The main function of each port has been described in detail in reference [33]. The state (open or closed) and ruler of the 10 ports are determined according to the instantaneous position of the moving components inside the corresponding valve. The moving position of the internal components of the valve is determined by the combined action of the corresponding instantaneous piston pressure, spring pressure and friction force on the inner wall of the valve.

The calculation of air-flow in braking system mainly includes the calculation of pressure in pipeline and chamber. Based on the momentum conservation, energy conservation and mass conservation, the following equations in pipe are obtained:

$$\begin{cases} \dfrac{\partial \rho}{\partial t} + \rho \dfrac{\partial u}{\partial x} + u \dfrac{\partial \rho}{\partial x} + \dfrac{\rho u}{F} \times \dfrac{dF}{dx} = 0 \\ \dfrac{\partial u}{\partial t} + u \dfrac{\partial u}{\partial x} + \dfrac{1}{\rho} \dfrac{\partial p}{\partial x} + \dfrac{4f}{D} \times \dfrac{u^2}{2} \times \dfrac{u}{|u|} = 0 \\ \dfrac{\partial p}{\partial t} + u \dfrac{\partial p}{\partial x} - a^2 \dfrac{\partial \rho}{\partial t} - a^2 u \dfrac{\partial \rho}{\partial t} - (k-1)\rho \left(q + u \dfrac{4f}{D} \times \dfrac{u^2}{2} \times \dfrac{u}{|u|} \right) = 0 \end{cases} \tag{7}$$

In these equations, ρ, u and p are the gas density, velocity and pressure respectively, a is the sound velocity, D, F and f are the hydraulic diameter of the fluid cross-sectional area of the tube and friction coefficient of the inner wall of the tube respectively. k, q, x and t are the gas-specific heat ratio, heat exchange quantity per unit time, distance and time respectively [25].

The physical quantities of each gas are transformed into Riemann variables and entropy expressions. After dimensionless transformation, three characteristic line directions and corresponding incremental expressions can be obtained:

Along the λ characteristic line:

$$\begin{aligned} d\lambda = {} & \frac{A}{A_A} dA_A - \frac{k-1}{2} \frac{AU}{F} \frac{dF}{dX} dZ + \frac{(k-1)^2}{2} \frac{qX_{ref}}{a^3{}_{ref}} \frac{1}{A} dZ \\ & - \frac{k-1}{2} \frac{2fX_{ref}}{D} U^2 \frac{U}{|U|} \left[1 - (k-1) \frac{U}{A} \right] dZ \end{aligned} \tag{8}$$

Along the β characteristic line:

$$\begin{aligned} d\beta = {} & \frac{A}{A_A} dA_A - \frac{k-1}{2} \frac{AU}{F} \frac{dF}{dX} dZ + \frac{(k-1)^2}{2} \frac{qX_{ref}}{a^3{}_{ref}} \frac{1}{A} dZ \\ & + \frac{k-1}{2} \frac{2fX_{ref}}{D} U^2 \frac{U}{|U|} \left[1 - (k-1) \frac{U}{A} \right] dZ \end{aligned} \tag{9}$$

The characteristic line along the entropy trace:

$$dA_A = \frac{k-1}{2}\frac{A_A}{A^2}\left[\frac{qX_{ref}}{a_{ref}} + \frac{2fX_{ref}}{D}|U|^3\right]dZ \tag{10}$$

Where, λ and β are Riemann variables, A_A is entropy, X, Z, U, A and F are dimensionless distance, dimensionless time, dimensionless velocity, dimensionless sound velocity and dimensionless area respectively. X_{ref} and a_{ref} are specific heat ratio, reference length and reference sound velocity respectively [35].

The system limit equations are as follows:

(1) The closed-end limit equation is mainly used for the end of pipelines, such as the end of the train pipe. The equation is as follows:

$$u = 0 \tag{11}$$

(2) The limit equation of the partial opening end is mainly used for the exhaust of the train pipe during emergency braking and service braking. The equation is as follows:

$$[(A*)^{4/(k-1)}](\lambda * -A*)^2 - \frac{k-1}{2}\phi^2[(A*)^2 - 1] = 0 \tag{12}$$

(3) The multi-branch limit equation of pipelines is mainly used at the junction of the main pipe and the branch pipe. The equation is as follows:

$$A_N^* = \frac{\sum_{j=1}^{N} F_j\left[\frac{\lambda_j^*}{A_{0,j}}\right]}{\sum_{j=1}^{N}\left[\frac{F_j}{A_{0,j}}\right]} = \left[\frac{p_i}{p_r}\right]^{(k-1)/2k} \tag{13}$$

$$U_i^* = \frac{2}{k-1}[\lambda_i^* - A_i^*] \tag{14}$$

(4) The limit equation of train pipeline resistance is mainly used to simulate hose connectors, and the equation is as follows:

$$\frac{\frac{2}{k-1} + M_2^2}{\frac{2}{k-1} + M_1^2} = \frac{M_1^2}{M_2^2(1 - KM_1^2)} \tag{15}$$

(5) The limit equation at the junction of brake cylinders and a train pipeline is as follows:

$$\frac{p_p}{p_c} = \left\{\begin{matrix} \varphi\left[\frac{2}{k+1}\right]^{(k+1)/[2(k-1)]}\left[1 - \frac{k-1}{2}U^2\right]\frac{1}{U} & u = a \\ \left\{\frac{1}{2C}\left[\varphi\sqrt{\varphi^2 + 4C} - \varphi^2\right]\right\}^{k/(k+1)} & u < a \end{matrix}\right\} \tag{16}$$

where U is the dimensionless flow velocity, ϕ and φ are the pipe opening area ratio and the cylinder opening area ratio respectively. M_1 and M_2 are the Mach numbers of upstream and downstream respectively. p_c, p_p and p_r are in-cylinder gas pressure, pipe pressure and

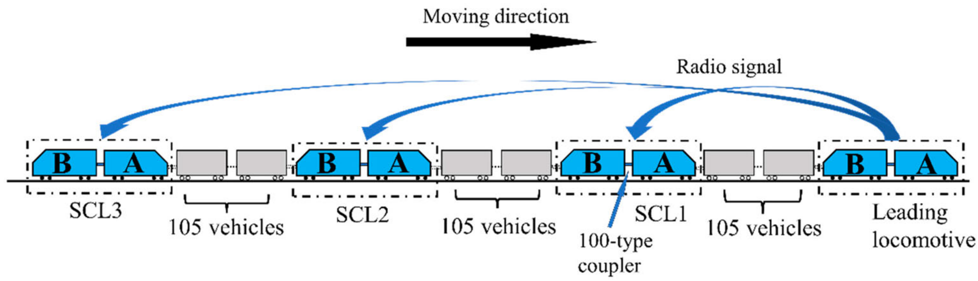

Figure 3. Formation of the 30,000-ton combined train.

reference pressure respectively. C and N are the coefficients related to the flow rate with one dimension and the number of connecting pipe joints, respectively. The variables with subscripts i and j are the corresponding variables of this variable in multi-branch pipelines. The variable with $*$ indicates the corresponding variable divided by the entropy value [36].

3. Verification of model

As shown in Figure 3, the 30,000-ton combined train consists of one leading locomotive, three slave control locomotives (SCL1, SCL2 and SCL3) and 315 C80B vehicles, and adopting a distributed power mode. The test train is equipped with LOCOTROL wireless synchronous control system. Every three vehicles are assembled with drawbars to form a group. The wagon groups are connected with 17-type couplers and equipped with 120-type brake and MT-2 type draft gear. A normal MT-2 draft gear is installed behind the drawbar. The formation of the test train is as follows: leading locomotive(2∗HXD1)+105∗C80B+SCL1(2∗HXD1)+105∗C80B+SCL2(2∗HXD1)+105∗C80B+SCL3(SS4G)(1+1+1+1 marshalling).

The static test consists of three test contents: train pipe pressure, brake cylinder pressure and auxiliary reservoir pressure. The constant pressure of train pipe is set to 600kPa. The test section positions of the first 10,000-ton unit are at 1, 25, 46, 61, 79 and 105 (positions in the middle of the unit) respectively. The test section positions of the second 10,000-ton unit are 1, 25, 52, 79 and 105 respectively. The test section positions of the third 10,000-ton unit are 1, 25, 53, 79 and 105 respectively. The test equipment of the test vehicles is equipped with a GPS antenna to ensure that all data collection times are synchronised to the same time axis [37].

3.1. Comparison between test and simulation

Table 1 shows the average value of the vehicle's brake cylinder balance pressure and the simulation comparison results. The maximum error does not exceed 2.0%. Taking pressure reduction of 100 kPa as an example, the three test and simulation results are shown in Figure 4. Due to the influence of various components of the vehicle braking system, the brake cylinder pressure of vehicles with different sections exhibits a certain random distribution. There are significant differences in the test results of brake cylinder balance pressure for individual vehicles.

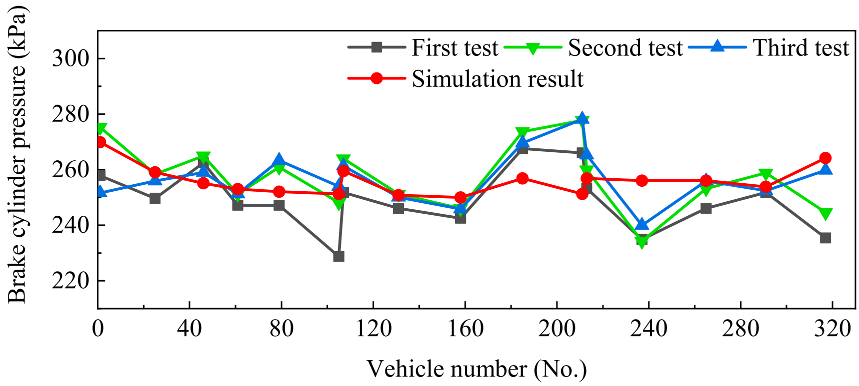

Figure 4. Brake cylinder pressure of each section.

Table 1. Comparison of average brake cylinder pressure results.

Pressure reduction	Test result/kPa	Simulation result/kPa	Error
50kPa	108.4	106.4	1.8%
70kPa	157.7	158.4	0.4%
100kPa	257.6	256.0	0.6%
170kPa	458.5	452.4	1.3%
Emergency braking	457.7	452.4	1.2%

The results of the train's initial braking synchronisation are shown in Figure 5(a). Under service braking conditions, when the train is in normal communication, the entire train can produce the braking effect within 8s after the leading locomotive implements braking. The LOCOTROL transmission delay of the three tests is less than 2.5 s. The vehicle with the slowest braking may appear in the middle of the second or third 10,000-ton unit.

Figure 5(b) shows the result of the initial braking synchronisation of emergency braking. In the first static test, the LT of the SCLs is slightly longer due to factors such as network operation state and external interference. The results of the last two tests are relatively normal. Except for the first test, the SCLs' LT is less than 1.5 s. All vehicles in the middle of the first 10,000-ton unit are braked within 5 s, and the slowest braking vehicle may appear in the middle of the second or third 10,000-ton unit. It can be seen from the figure that the simulation results are in better agreement with the test data.

Figure 6 shows the results of the simulation and test on the onset release time of brake cylinders in various sections under service braking conditions. The transmission delay of the three tests is about 2 ~ 3 s. All vehicles can produce release effect within 8s. The vehicle with the slowest release may appear in the middle of the second or third 10,000-ton unit.

The longest time for charging the auxiliary reservoir pressure of vehicles with various sections to 580 kPa after the train is braked is defined as the recharging time. The recharging times of the test and simulation is shown in Table 2. Similar to braking conditions, theoretically, the middle vehicles of the second and third 10,000-ton units will be slightly slower to charge air. The error between the simulation results and the test results is within 4%.

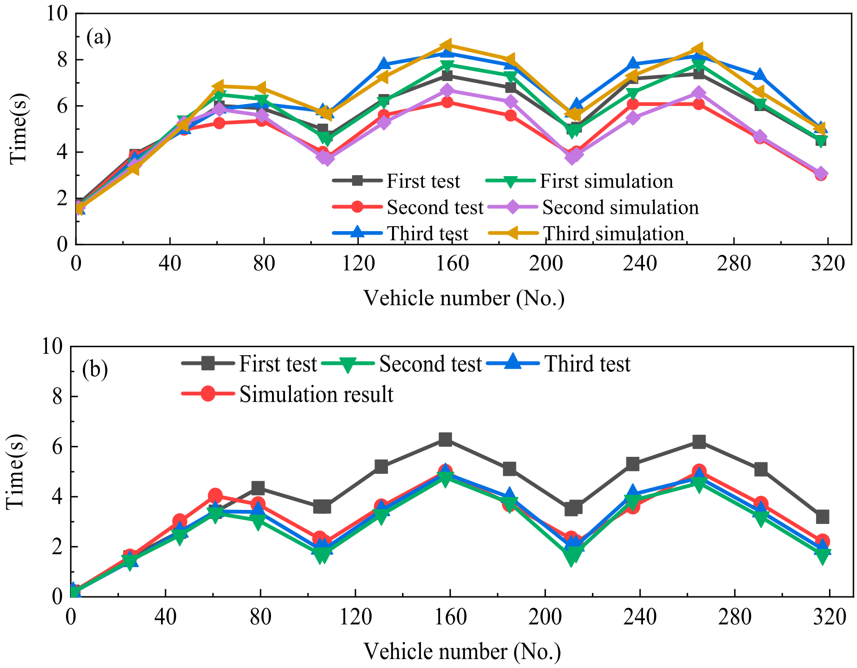

Figure 5. Brake cylinder exit time of each section for initial braking: (a) service braking and (b) emergency braking.

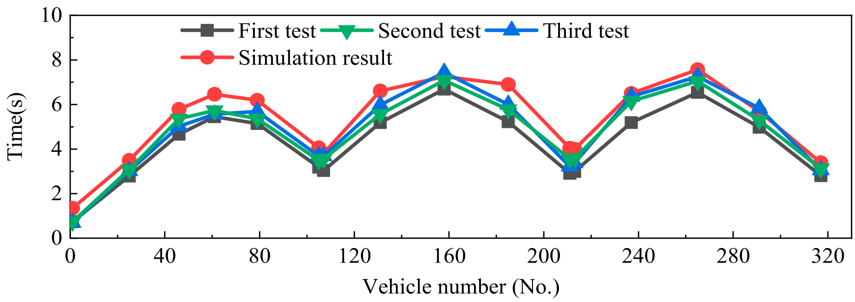

Figure 6. Onset release time of each section under service braking conditions.

Table 2. Comparison of recharging time results.

Pressure reduction	Last wind-filled section	Test result/s	Simulation result/s	Error
50 kPa	157	65	66	2.0%
70 kpa	184	91	90	1.0%
100 kPa	130	142	138	2.8%
170 kPa	157	205	197	3.9%

Through the comparison of the above simulation and test results, the validity of the air brake system model of the simulation system is verified, and the accuracy of the 30,000-ton combined train model is confirmed.

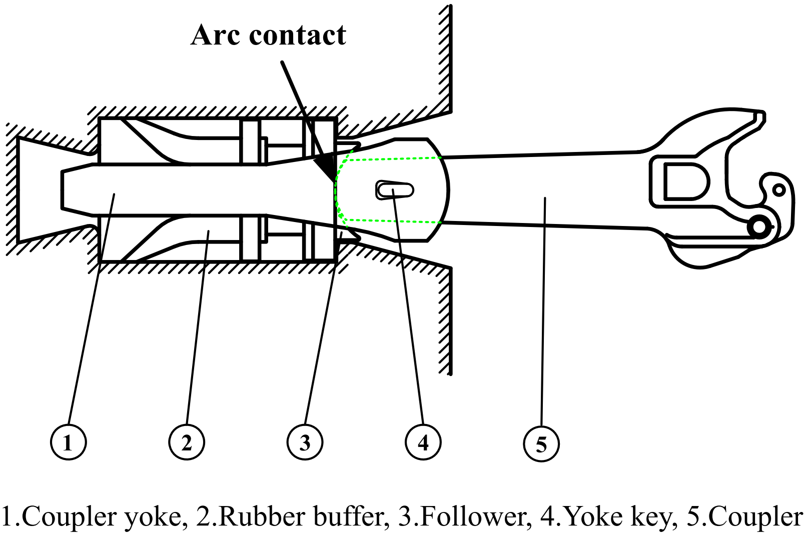

Figure 7. Structure diagram of the 100-type coupler. 1. Coupler yoke, 2. Rubber buffer, 3. Follower, 4. Yoke key, 5. Coupler.

4. Model of 100-type coupler

4.1. Coupler structure

At present, the couplers of heavy-haul locomotives in China can be roughly divided into two types according to the structural types: the first type of couplers has arc contact with unequal radii at the tail end, and the smaller lateral force of couplers is realised skilfully through mechanism movement. The second type prevents the coupler from turning at a large angle by setting a stop, so as to keep the coupler stable. The 100-type coupler belongs to the first type coupler, and its structure is shown in Figure 7. The key technology of this type of coupler is that the radii of the two arcs contacting the follower and the end of the coupler surface are different. When there is friction, the unequal radii make the two arcs roll instead of slide [38].

4.2. Stability mechanism

Figure 8 shows the contact analysis between the coupler-tail end and the arc surface of the follower. The radii of the two arc surfaces are different, so it can be assumed that the tail end of the coupler is in line contact with the follower. Due to the friction of the contact surface, the position of the contact point moves with the arc when the coupler is deflected. The contact angle β is the angle between the centre line of the follower and the contact point. Assuming that the friction of the contact surface is not saturated, the two arc surfaces are pure rolling, and the yaw angle α and the contact angle β satisfy the following relationship:

$$\beta = \frac{r}{R - r}\alpha \tag{17}$$

Where, r and R are the respective radii of the end of the coupler and the follower.

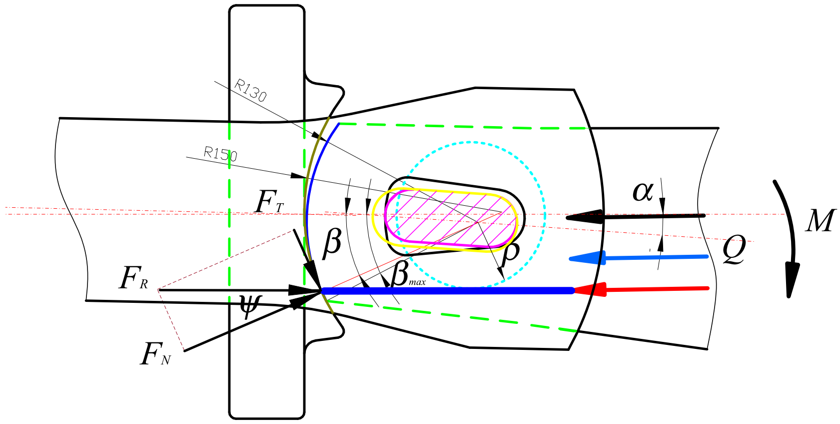

Figure 8. Contact analysis of the end arc surfaces.

During the braking process, the train will produce a large compression coupler force, so that there is a relative lateral movement between the car bodies at both ends of the coupler. The coupler is subjected to the longitudinal compression force Q and the deflection torque M along the direction of the coupler. M can be equivalent to the translation distance L of Q in the direction of the vertical force line, where $L = M/Q$. Based on the friction circle theory, the detailed process of force analysis of the coupler can be referred to reference [17]. The friction circle is made at the centre of the arc at the tail end of the coupler, and the radius is ρ. There is the following relationship between ρ and the friction coefficient μ of the two arc contact surfaces:

$$\rho = r\sin(\tan^{-1}\mu) \tag{18}$$

This paper mainly describes the process of coupler from stability to instability. In this process, the arc contact surface goes from pure rolling to sliding states, and the coupler yaw angle α and the contact angle β go through two states:

The first stage: assuming that the initial the coupler yaw angle is 0°, when the coupler yaw angle α increases, the contact angle β increases. When the coupler yaw angle increases to a certain extent, the contact surface friction reaches saturation. As shown in Figure 9 (1), the force transmission line (the line connecting the arc contact points at both ends of the coupler) generated in this stage is located in the inner common tangent of the friction circle at both ends of the coupler. At this time, the lateral relative displacement y_c of the car body at both ends does not exceed the critical lateral displacement Y_{bc}. The force transmission line is parallel to the track direction, and the lateral force of the coupler is 0.

The second stage: As shown in Figure 9(2), after exceeding the critical state, when α increases, β decreases. At this time, the lateral displacement of the car body continues to increase, the adhesion state between the two contact surfaces changes from stick to slip in the opposite direction, and the angle of the force transmission line is greater than 0. A large coupler yaw angle will generate a large coupler lateral force, which will be transmitted to the car body and the car body to the bogie, which will make the wheelset lateral force increase sharply and affect the safety of train operation.

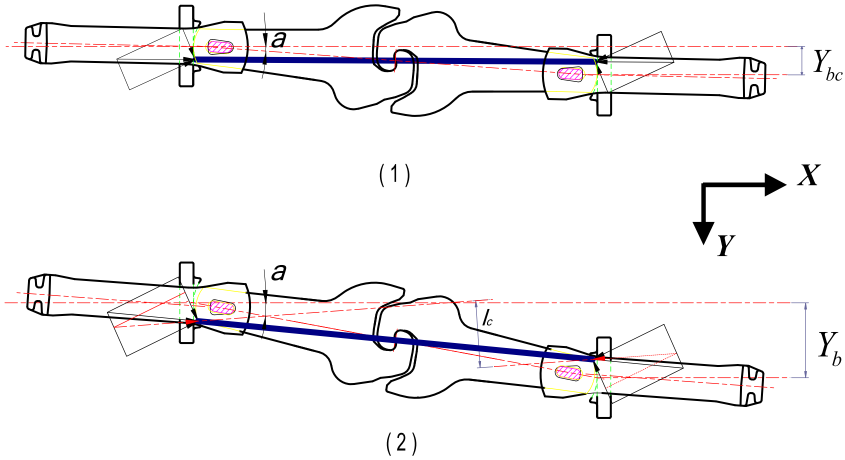

Figure 9. Two states of force transmission line.

Table 3. Parameters of the locomotive HXD1 and the wagon C80B.

Parameter	HXD1	C80B
Length at coupling line (m)	17.611	12
Bogie spacing (m)	9	8.2
Coupler length (m)	0.824	0.735
Axle load (t)	25	25
Maximum velocity (km/h)	120	120
Total weight (t)	100	100
Coupler type	13A	16-Type rotary dump coupler, 17-type fixed coupler

5. Influence of LT of SCLs on longitudinal impulse

In the following study, the 30,000-ton combined train configuration is as follows: leading locomotive (2∗HXD1) + 105∗C80B + SCL1(2∗HXD1) + 105∗C80B + SCL2(2∗HXD1) + 105∗C80B + SCL3(SS4G). HXD1 is the locomotive model, and C80B is the vehicle model. The C80B vehicles are equipped with the 120 distributing valve and the HM-1 type draft gear. Table 3 lists some parameters of the HXD1 and the C80B. The drawbars are used between vehicles, with 2 vehicles forming a group. A normal HM-1 type draft gear is installed behind each drawbar. The train is set to make emergency braking on the flat straight at a speed of 70 km/h. No track excitation is considered. The brake pipe pressure is 600 kPa. The LT of the SCLs ranges from 0-6 s, with an interval of 1 s. No electric braking force is applied during the simulation calculation. Meanwhile, according to 'Standard on Strength and Accreditation Test of Railway Vehicles: TB/T 1335-1996', the limit value of coupler force for emergency braking should not exceed 2250 kN [39].

5.1. Simulation result analysis

5.1.1. LT of SCLs is consistent

Figure 10 shows the distribution of the maximum coupler force of each coupler on the train when the SCLs' LT is 0 s. The positive value represents the tensile coupler force, and the negative value represents the compression coupler force. The maximum compression

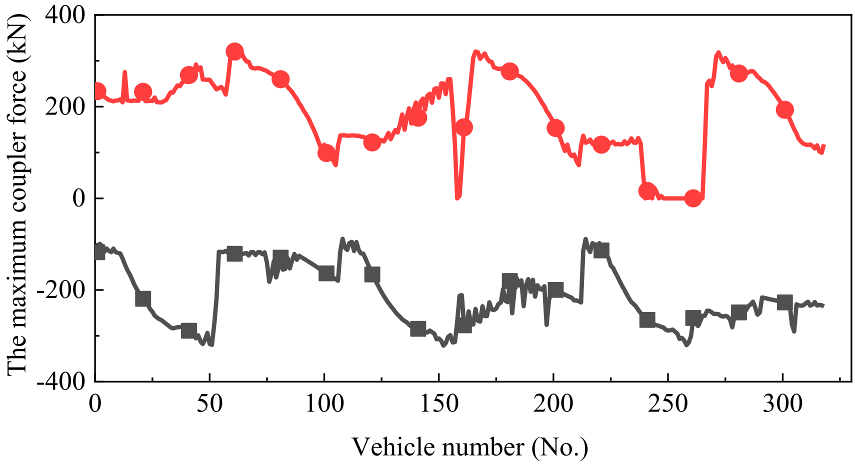

Figure 10. Distribution of the maximum coupler force when the LT is 0 s.

and tensile coupler force are −321.4 and 320.2 kN, respectively. The maximum value of the tensile coupler force is close to the maximum compression coupler force. It can be seen that the distribution of the maximum coupler force is divided into three parts by four locomotives, and the distribution law of the coupler force in each part is similar, the coupler force increases first and then decreases. The maximum coupler force peak is in the middle of two adjacent locomotives, and this position is at the abrupt change of coupler force distribution.

Figure 11 shows the distribution curve of the maximum coupler force on the train when the SCLs have LT. As the LT increases, the distribution pattern of the maximum coupler force changes, and the maximum coupler force peak shifts from the middle position of the original two adjacent locomotives to the middle position of the entire train. For the maximum tensile coupler force distribution, the gradient of change is steep near the middle locomotive position, and the gradient of the maximum compression coupler force distribution at this position is not very obvious. With the increase of the LT, the compression coupler force of the train is obviously greater than the tensile coupler force. The compression coupler force will increase sharply when the LT of the SCLs exceeds 2 s, and the tensile coupler force will increase sharply when the LT exceeds 3 s. The LT from 2 s to 3 s, and the maximum compression coupler force increases from 757.8 kN to 1721.5 kN.

The LT of SCLs from 0 s to 6 s, and the maximum compression coupler force increased from 321.4 kN to 2198.5 kN, an increase of 1877.1 kN. The safety margins of the maximum coupler force corresponding to the LT of 5 s and 6 s are 13.9% and 2.3% respectively, and the maximum coupler force is located near the first SCL. Therefore, in order to ensure the normal and safe operation of the 30,000-ton combined train, the LT of the SCLs should be controlled within 5 s.

5.1.2. LTs of SCLs are inconsistent

It is very difficult to determine which SCL's LT has the greatest influence on the maximum coupler force in the test, which requires high risk and cost. There is no doubt that

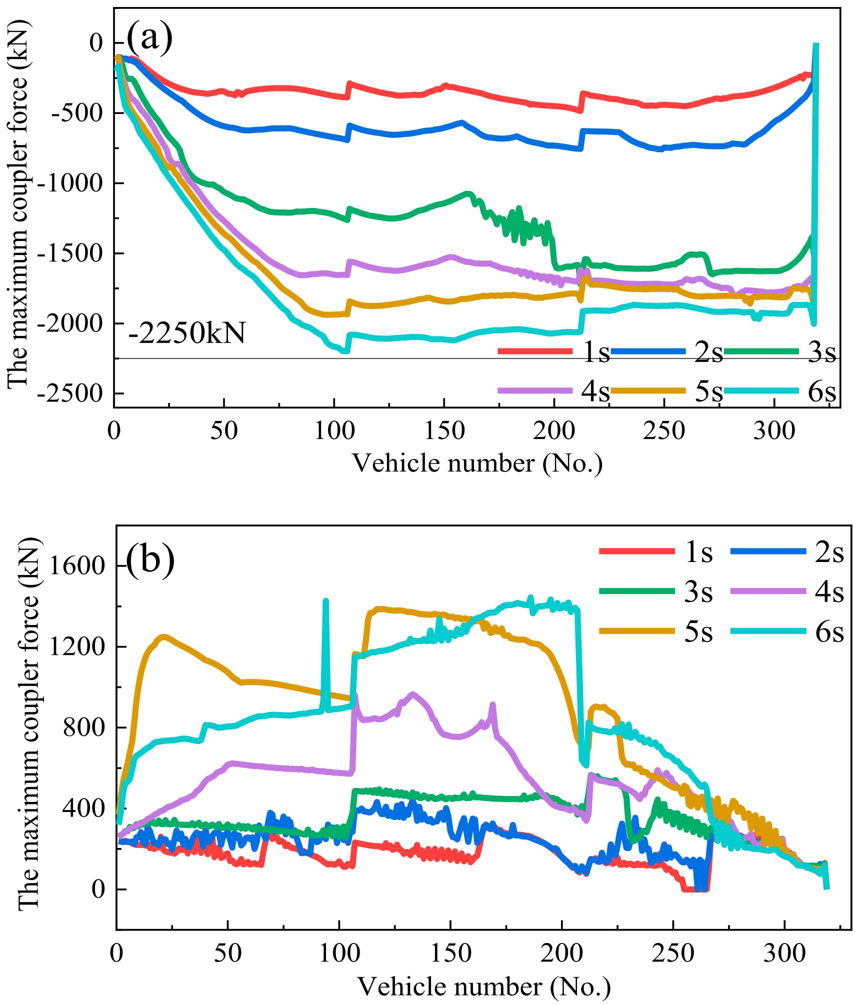

Figure 11. Maximum coupler force distribution: (a) maximum compression coupler force and (b) maximum tensile coupler force.

it is of great significance to get the corresponding results by means of simulation before the formal test. In this section, the LTs of the three SCLs are inconsistent. The LT of one SCL with poor communication delay is 6 s, while the communication delay of the other two SCLs is 2 s. Thus, there are three combinations: 6-2-2 (where the LT of SCL1, 2 and 3 are 6 s, 2 s and 2 s respectively), 2-6-2 and 2-2-6. Each combination is calculated once.

Figure 12 shows the piston action time of each vehicle brake cylinder during emergency braking, representing the braking wave transmission process. It can be seen that each segment is basically a straight line, indicating that the braking wave basically propagates at a constant speed during emergency braking. The brake wave transmission law of the combined train is as follow: the leading locomotive is transmitted from front to back. The middle of SCL transmits forward and backward, and the tail SCL is transmits forward.

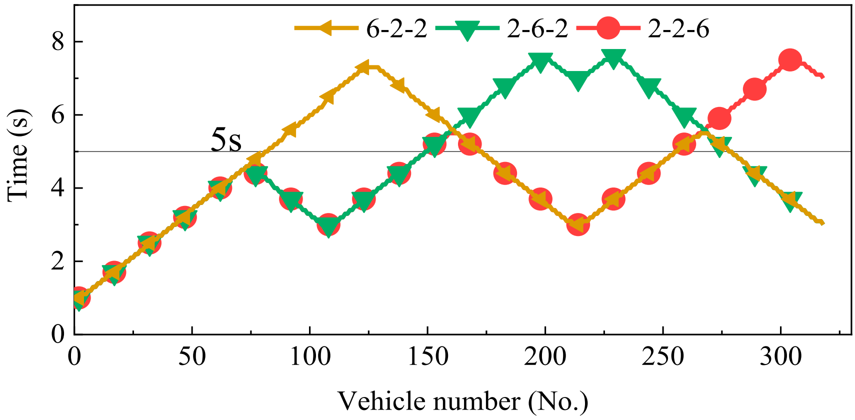

Figure 12. Curve of the transmission characteristics of the brake wave.

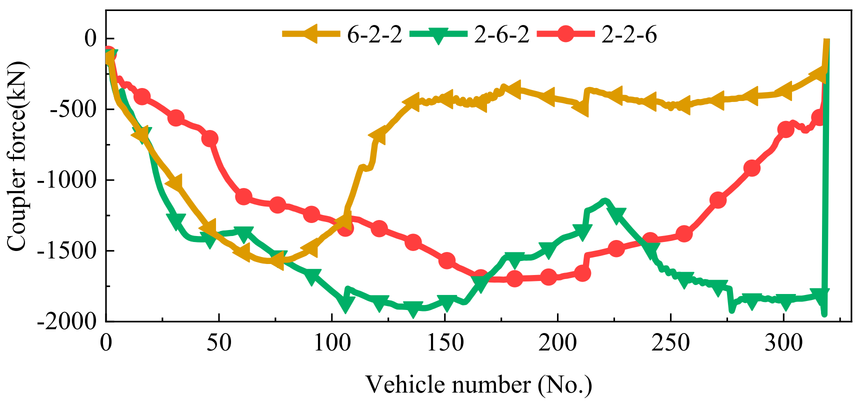

Figure 13. Distribution of the maximum coupler force on the train.

The number of vehicles with the start-up action time of the brake cylinder exceeding 5 s and the mean LT of these vehicles are taken as the analysis targets. For the combinations 6-2-2, 2-6-2 and 2-2-6, the number of vehicle brake cylinders that started to act for more than 5 s is 118, 130 and 88 respectively. The mean values of the excess part are 5.98, 6.51 and 6.13 s, respectively. That indicates that, under the same LT, the influence of SCL2 on the overall braking delay of the train is more significant. Consequently, the influence of SCL2 on the coupler force will also be more significant.

In Figure 13, the maximum compression coupler force corresponding to the three curves of 6-2-2, 2-6-2 and 2-2-6 is distributed along the train length. When the braking LT of SCL1 is large, it only has an obvious influence on the coupler force of the front 1/3 of the entire train, and has little influence on the rear 2/3 of the train. The SCL2 and 3 have a significant impact on the overall coupler force of the train. The maximum coupler forces corresponding to 6-2-2, 2-6-2 and 2-2-6 are 1572.5, 1950.0 and 1704.1 kN, respectively. That is, the influence ability of the LT of the SCL2 on the maximum coupler force

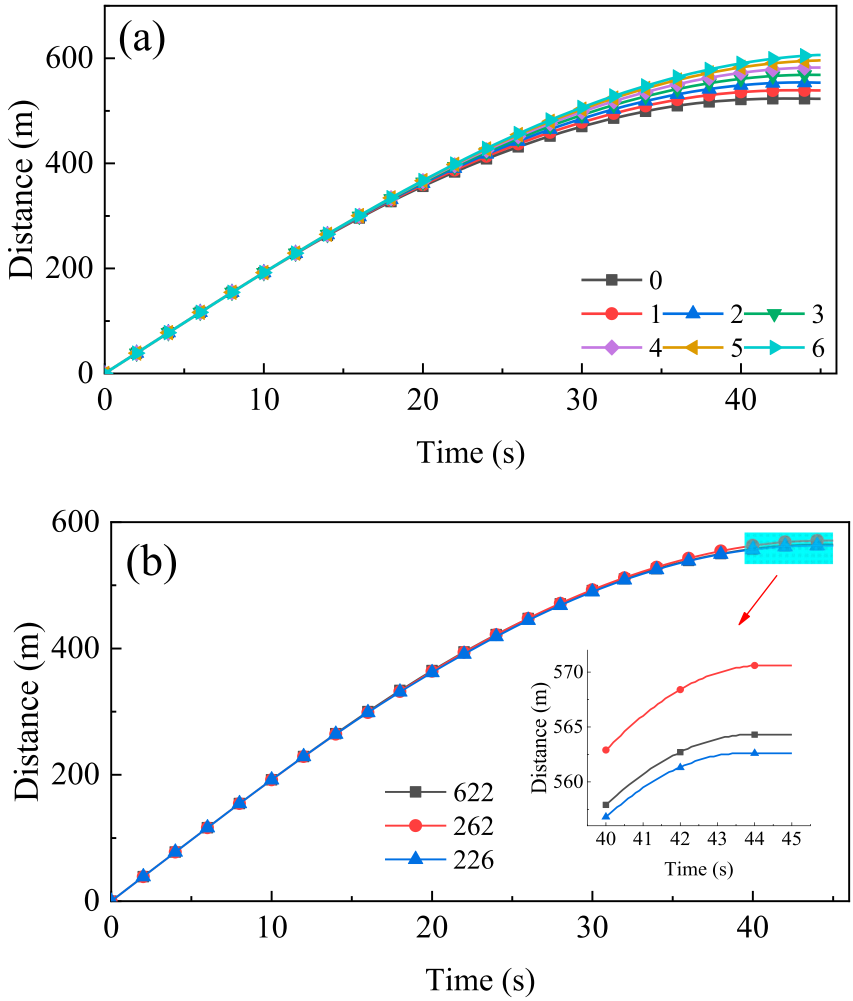

Figure 14. Emergency braking distance: (a) consistent LT of SCLs and (b) inconsistent LT .of SCLs

> SCL 3 > SCL1. The highest coupler force is in the vicinity to SCL1, and therefore the derailment risk is highest near SCL1.

5.1.3. Influence of the emergency braking distance

Figure 14 (a) is the time-domain curve corresponding to the emergency braking of the train when the LT of the SCLs is consistent. The LT of the SCLs has little effect on the braking distance. For every 1 s increase in the LT, the emergency braking distance increases by 10–15 m (the initial speed of the train is 70 km/h). Compared with the synchronous braking of the locomotives, the LT of the SCLs is 6 s, and the braking distance is increased by 15.9%, and the increase value is 83.4 m. Figure 14(b) is a time-domain curve when LT of SCLs is inconsistent. It can be seen that the SCL 2 has a greater impact on the train braking capacity than the other two SCLs. But these differences are very small and have little practical significance.

6. Operation safety analysis of middle locomotive

6.1. Dynamics model of locomotive and coupler

According to the actual locomotive parameters, a detailed dynamic model of HXD1 heavy-haul locomotive is established by using multi-body dynamics simulation software SIMPACK. The SCL is composed of two HXD1-type locomotives connected by a 100-type coupler. Its dynamic model is shown in Figure 15. The main suspension parameters of the locomotive are shown in Table 4. Calculating coupler force with different lag time by TABLDSS. The coupler forces at the front and rear ends of SCL1 are extracted as F1 and F2, respectively, and loaded into the front and rear ends of the model in SIMPACK. This method is simple and can meet the requirements of calculation accuracy.

6.2. Research object and calculation conditions

According to section 5.1, the maximum coupler force appears near the first SCL, so this section selects the first SCL as the research object. At the beginning time of the emergency brake, the train was running on a straight track at a speed of 70 km/h. The track irregularity in accordance with AAR5 [40]. The simulation time is 40 s, and the train speed is reduced

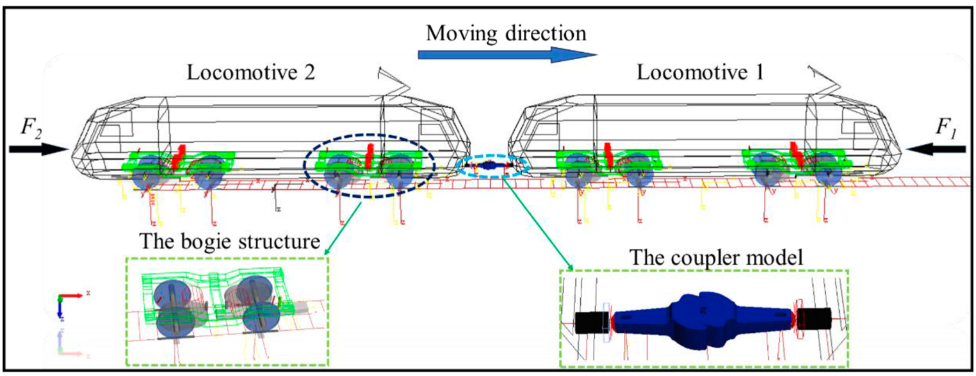

Figure 15. Dynamic simulation model of SCL.

Table 4. Main suspension parameters of the locomotive

Main parameter name	Value
Axle arrangement	2*B*0
Axle load (t)	25
Bogie spacing (m)	9
Length at coupling line (m)	17.611
Friction coefficient of arc contact pair	0.35
Height of coupler (m)	0.88
Radius of coupler-tail arc surface (mm)	130
Radius of following plate arc surface (mm)	150
Free clearance of secondary lateral stop (mm)	35
Elastic clearance of secondary lateral stop (mm)	5
Elastic stiffness of secondary lateral stop (kN/mm)	14
Lateral stiffness of secondary suspension (per side) (kN/mm)	0.696
Maximum free rotation angle of the coupler(°)	13

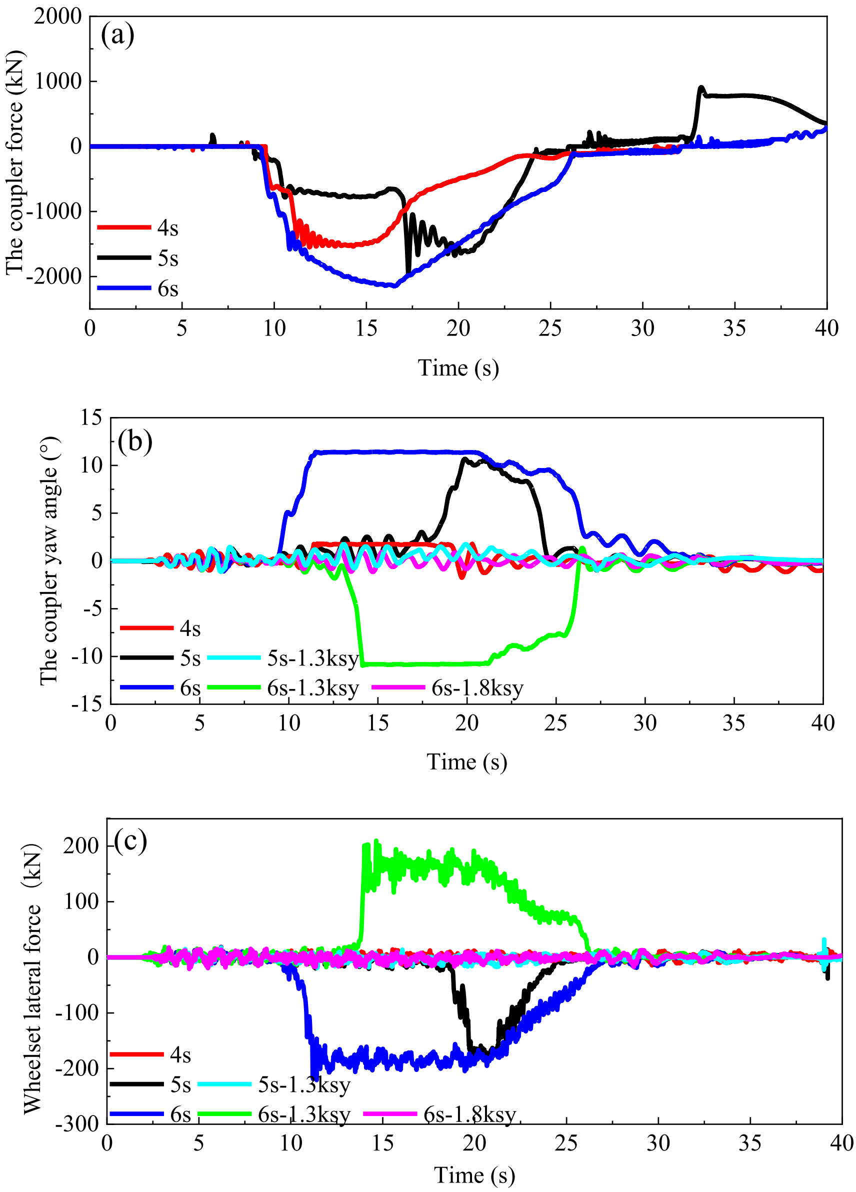

Figure 16. Time-domain results: (a) coupler force, (b) coupler yaw angle and (c) wheelset lateral force.

from 70 km/h to 0 km/h. In this section, the LT settings of the three SCLs are consistent. LT of each SCL is set to 4～6 s to simulate the poor communication conditions between SCLs and leading locomotive. In the following discussion, the stability of the coupler is evaluated by analysing the yaw angle of the coupler under compression. When the coupler has a large yaw angle, the coupler is in an unstable state. Note that in order to better compare the results, the wheelset lateral force of the fourth axle of the locomotive 1 is used to evaluate the running safety of the locomotive.

6.3. Simulation result analysis

Figure 16 shows the longitudinal force of the coupler in the middle locomotive, the yaw angle of the coupler and the wheelset lateral force under different LTs ('5 s-1.3 ksy' indicates that the LT of the SCLs is 5 s and the lateral stiffness of the secondary suspension is 1.3 times the original). When the LT of the SCLs is 4 s, the coupler yaw angle and the wheelset lateral force are small. That is to say, the LT of the SCLs is less than 4 s, and the application of the 100-type coupler on the 30,000-ton combined train can ensure the safety of train operation. It is worth noting that from the longitudinal dynamics study in Section 5.1, when the LT of SCLs is 5 s, there is still a safety margin of 13.6%. However, when the LT of the SCLs reaches 5 s, the coupler yaw angle of the middle locomotive reaches 10.4°, and the wheelset lateral force reaches 200 kN, which is an extremely dangerous state. Therefore, in order to ensure the safe operation of the 30,000-ton combined train, it is far from enough to analyse the value of the coupler force alone, and the lateral stability analysis of the coupler is also an essential part.

In Figure 16 (b) and (c), the lateral stiffness of the locomotive's secondary suspension is increased to 1.3 times the original, and the coupler yaw angle and the wheelset lateral force corresponding to the LT of 5 s are greatly reduced. When the lateral stiffness of the secondary suspension increases to 1.8 times, the LT of the SCLs reaches 6 s, the locomotive can also maintain the stability of the coupler. Note that when the LT is 6 s, the coupler cannot be stabilised when the locomotive matches 1.3 times the original lateral stiffness of the secondary suspension. However, the initial instability time of the coupler is delayed by about 5 s, and the coupler force corresponding to the initial instability of the coupler becomes larger. Therefore, increasing the lateral stiffness of the secondary suspension is a very effective measure to improve the locomotive's ability to stabilise the coupler.

The above results are mainly caused by the characteristics of the coupler. Through the theoretical analysis of Section 4, it can be seen that when the coupler is at a large yaw angle, the lateral component of the coupler force generated by the yaw angle of the force transmission line is balanced by the locomotive's secondary lateral suspension system. When the coupler's rotation torque is greater than the resistance torque caused by the locomotive's secondary suspension system, the coupler will be unstable. Because the coupler does not have the elastic stop function to limiting the small yaw angle, the instability of the coupler can cause a large lateral force on the coupler.

7. Conclusions

The longitudinal dynamic model of an expanded 30,000-ton combined train with '1+1+1+1' marshalling is established using Train Air Brake and Longitudinal Dynamics Simulation System (TABLDSS). The accuracy of the model is verified by comparing it with the static test of the train. Taking emergency braking as an example, the influence of the lag time (LT) of the slave control locomotives (SCLs) on train longitudinal impulse and the stability of the coupler in the middle of the SCL are studied. The following useful conclusions are made.

(1) The static test analysis of the 30,000-ton combined train shows that the vehicles with the slowest braking and release appear in the middle of the train. Under normal

transmission delays, the lag time in the braking response of the SCLs is approximately 2 ∼ 3 s,and all vehicles can generate braking force within 7s during emergency braking.

(2) The LT of braking response of the SCLs has a great influence on the coupler force and its distribution law, but has little influence on the braking distance. When the LT exceeds 2 s, a larger coupler force will be generated. The maximum coupler force increases by 1877.1 kN when the LT increases from 0 s to 6 s. In order to ensure the safe operation of the train, it is necessary to strictly control the LT within 5 s.

(3) The LT of the SCL located in the middle of three SCLs has the greatest influence on the coupler force. The LT of the SCL in this position has significantly impacts on the overall braking delay of the train and the largest number of vehicles, which increases the forward impact level on some vehicles when the train brakes, thereby generating greater coupler force. In addition, the SCL near the leading locomotive has little influence on the longitudinal impulse level of the entire train.

(4) When the LT of the SCLs reaches 5 s, the coupler of the middle locomotive is unstable. Increasing the lateral stiffness of the secondary suspension is a very effective measure to enhance the locomotive's ability to stabilise the coupler.

Disclosure statement

No potential conflict of interest was reported by the author(s).

Funding

This paper is based on the National Natural Science Foundation of China [grant numbers 52372403; U2268211], the Sichuan Provincial Natural Science Foundation [grant number 2022NSFSC0034], and the National Railway Group Science and Technology Program [grant number N2023J071].

ORCID

Yuan Yao http://orcid.org/0000-0003-2279-7463

References

[1] Chong YC, Gang G, Wen H, et al. Simulation study on the influence of longitudinal dynamic force on extreme-long heavy-haul trains. Railw Sci. 2023;2(4):495–513.

[2] Yao XP, Guo XY, Xiong X, et al. Test of 30,000-ton heavy-haul combined train and suggestions on optimum operation. China Railw. 2022;1(11):39–44.

[3] Zhao X, Wang CG, Ma DW. Influence of locomotive wireless sync control technology on the longitudinal force of 20,000 t heavy combined train. China Railw Sci. 2008;29(3):78–83. Chinese.

[4] He W, Chang ZY, Wang JB, et al. Analysis on key influencing factors of longitudinal force with 30 000 t heavy haul trains in braking conditions. J China Railw Soc. 2024;46(1):53–55. Chinese.

[5] Xin G, Liang L, Zai GC, et al. Experimental assessment of the dynamic performance of slave control locomotive couplers in 20,000-tonne heavy-haul trains. Proc Inst Mech Eng Part F J Rail Rapid Transit. 2021;235(10):1225–1236.

[6] Rao JS, Raghavacharyulu E, Kumar N. Mathematical modelling to simulate the transient dynamic longitudinal force in draw bars of a train-consist. J Sound Vib. 1984;94(3):365–379.

[7] Geike T. Understanding high coupler forces at metro vehicles. Veh Syst Dyn. 2007;45(4): 389–396.

[8] Belforte P, Cheli F, Diana G, et al. Numerical and experimental approach for the evaluation of severe longitudinal dynamics of heavy freight trains. Veh Syst Dyn. 2008a;46(sup1):937–955.
[9] Cole C, Spiryagin M, Wu Q, et al. Modelling, simulation and applications of longitudinal train dynamics. Veh Syst Dyn. 2017;55(10):1498–1571.
[10] Wei W, Hu Y, Wu Q, et al. An air brake model for longitudinal train dynamics studies. Veh Syst Dyn. 2017;55(4):517–533.
[11] Wei W, Zhao JB, Jiang Y, et al. The integrated model of train air and longitudinal dynamics. J China Railw Soc. 2006;27(5):104–109.
[12] Simson SA, Cole C. Simulation of traction curving for active yaw-force steered bogies in locomotives.proc inst mech Eng part F. J Rail Rapid Transit. 2009;223(1):75–84.
[13] Luo SH, Feng QB, Yang JJ. Research on dynamics of the HXD2 heavy-load locomotive bearing longitudinal compressive strength. Railw Locomotive Car. 2008;28(S1):145–148+177. Chinese.
[14] Ma WH, Luo SH, Song RG. Coupler dynamic performance analysis of heavy haul locomotives. Veh Syst Dyn. 2012;50(9):1435–1452.
[15] Wu Q, Luo SH, Ma WH, et al. Modelling of coupler system for heavy-duty electric locomotive. Railw Locomotive Car. 2012;32(4):15–19. Chinese.
[16] Yao Y, Liu X, Zhang HJ, et al. The stability and mechanical characteristics of heavy haul couplers with restoring bumpstop. Veh Syst Dyn. 2013;52(1):26–44.
[17] Yao Y, Zhang XX, Zhang HJ, et al. The stability mechanism and its application to heavy-haul couplers with arc surface contact. Veh Syst Dyn. 2013;51(9):1324–1341.
[18] Yao Y, Zhang XX, Zhang HJ. Dynamic performances of an innovative coupler used in heavy haul trains. Veh Syst Dyn. 2014;52(10):1288–1303.
[19] Wang KY, Zhai WM, Feng QB, et al. Effect of the coupler free angle on wheel/rail dynamic safety performance of heavy haul locomotive. China Railw Sci. 2009;30(6):72–76.
[20] Shi Z, Wang K, Guo L, et al. Effect of arc surfaces friction coefficient on coupler stability in heavy haul locomotives: simulation and experiment. Veh Syst Dyn. 2017;55(9):1368–1383.
[21] Wu Q, Cole C, Spiryagin M, et al. Freight train air brake models. Int J Rail Transp. 2023;11(1):1–49.
[22] Oprea RA, Cruceanu C, Spiroiu MA. Alternative friction models for braking train dynamics. Veh Syst Dyn. 2013;51(3):460–480.
[23] Bosso N, Magelli M, Zampieri N. A numerical method for the simulation of freight train emergency braking operations based on the uic braked weight percentage. Railw Eng Sci. 2023;31(2):162–171.
[24] Pfaff R. Braking distance prediction for vehicle consist in low-speed on-sight operation: a monte carlo approach. Railw Eng Sci. 2023;31(2):135–144.
[25] Wei W, Zhang Y, Zhang J, et al. Influence of quick release valve on braking performance and coupler force of heavy haul train. Railw Eng Sci. 2023;31(2):153–161.
[26] Ge X, Chen Q, Ling L, et al. An approach for simulating the air brake system of long freight trains based on fluid dynamics. Railw Eng Sci. 2023;31(2):122–134.
[27] Pugi L, Rindi A, Ercole AG, et al. Preliminary studies concerning the application of different braking arrangements on Italian freight trains. Veh Syst Dyn. 2011;49(8):1339–1365.
[28] Gialleonardo DE, GazzulaniG, Melzi S, et al. The effect of train composition on the running safety of low-ffatcar wagons in braking and curving manoeuvres. Proc Inst Mech Eng Part F J Rail Rapid Transit. 2017;231(6):666–677.
[29] Cantone L. Traindy: the new union international des chemins de fer software for freight train interoperability. Proc Inst Mech Eng Part F J Rail Rapid Transit. 2011;225(1):57–70.
[30] Belforte P, Cheli F, Diana G, et al. Numerical and experimental approach for the evaluation of severe longitudinal dynamics of heavy freight trains. Veh Syst Dyn. 2008b;46(S1):937–955.
[31] Wu Q, Spiryagin M, Cole C, et al. International benchmarking of longitudinal train dynamics simulators: results. Veh Syst Dyn. 2018;56(3):343–365.
[32] National Railway Administration of the People's Republic of China. Railway train traction calculation part 1: trains with locomotives (TB/T 1407.1-2018). Beijing: China Railway Publishing House; Chinese.

[33] Yuan ZY. Research on rolling resistance of the shuo-huang heavy railway. [master's thesis]. Dalian: Dalian Jiaotong University; 2019. Chinese.
[34] Wei W, Li WH. Simulation of a freight train brake system with 120 valves. Proc IMechE Part F:Journal of Rail and Rapid Transit. 2009;223(1):85–92.
[35] Ma Q, Yao Y, Meng FY, et al. The design of electronically controlled pneumatic brake signal propagation mode for electronic control braking of a 30,000-ton heavy-haul train. Proc Inst Mech Eng Part F J Rail Rapid Transit. 2024;238(2):268–279.
[36] Wei W, Zhao JB, Jiang Y, et al. The integrated model of train air brake and longitudinal dynamics. J China Railw Soc. 2012;34(4):39–46. Chinese.
[37] Yu Y. Longitudinal dynamics simulation research of 30,000 t heavy-haul trains on shuohuang railway [master's thesis]. Dalian: Dalian Jiaotong University; 2023. Chinese.
[38] Wu GS, Wang H, Yao Y. Improvements for the stability of heavy-haul coupler with arc surface contact. Veh Syst Dyn. 2018;56(3):428–442.
[39] Ministry of Railways of the People's Republic of China. Standard on strength design and accreditation test of railway vehicles: TB/T 13335-1996. Beijing: Chian Railway Publishing House. Chinese.
[40] Zhai WM. Vehicle-Track coupler dynamics, 3rd ed. Beijing: Science Press; 2007; ISBN 978-7-03-018326-2, Chinese.